2D Laser-Induced Phased Arrays for Large-Area Scans Using Poisson-Disk Layouts

MOHAMMAD ALI FAKIH, SERGIO CANTERO-CHINCHILLA, ANTHONY CROXFORD and PAUL D. WILCOX

ABSTRACT

There is an increased need for the development of reliable non-contact non-destructive evaluation (NDE) techniques which can be deployed using machines/robots in remote locations and risk-associated environments. This work suggests a new ultrasound scanning technique for large areas using 2D laser-induced phased arrays (LIPAs). The objective is to achieve a given detection sensitivity using the smallest possible number of measurements. This reduces the scanning time, size of the collected data, and energy usage. Bridson Poisson sampling is proposed to define both the generation-laser aperture relative to a single detection point (physical aperture) and the detection-laser scanning points over an arbitrary inspection surface. The proposed imaging solution is based on the total focusing method (TFM) but differs from conventional and previous LIPA solutions. The full matrix capture (FMC) for each imaging location on the surface, referred to as the region of interest (ROI), is determined by the available detection points within its vicinity. This vicinity is expressed by a specific radius, defining the size of the computational aperture. The proposed methodology is analytically evaluated using ray-tracing model simulations. Poisson-disk sampling is compared to regular-shaped (square and triangular) grids, demonstrating its clear superiority in both detection/imaging performance and scanning time. Recommendations for optimisation and experimental validation are suggested for future work.

I. INTRODUCTION

As our structures age or become more complex, the demand increases for non-destructive evaluation (NDE) techniques that are suitable for remote locations (e.g., offshore wind farms), extreme environments (e.g., high temperatures, radioactivity), or those with restricted or risk-associated access (e.g., nuclear power plants, wind-turbine fans, steel bridges). This necessitates the development of reliable, portable, and non-contact NDE technologies that can be deployed via inspection drones or robots. In this

School of Electrical, Electronic and Mechanical Engineering, University of Bristol, Bristol, BS8 1TR, UK

context, ultrasonic inspection using 2D laser-induced phased arrays (LIPAs) emerges as a promising solution.

The concept of LIPAs was introduced in [1] and successfully used in several applications. However, the lengthy acquisition time of this technique remains a concern that needs to be addressed. In a previous work, Cantero-Chinchilla et al. [2] suggested an optimisation framework to balance the defect detectability and acquisition time for 1D LIPAs. Efficient evaluation metrics were proposed for both detection and time, and multiple candidate LIPA configurations were evaluated. A set of recommendations was finally provided for omnidirectional and directional defects.

One-dimensional arrays enable cross-sectional 2D imaging of the inspected component but lack the ability to resolve the third spatial dimension, which is essential for a more accurate visualisation of internal features/defects [3]. This limitation can be addressed by employing 2D arrays, capable of capturing wave reflections away from the imaging plane of a 1D array [4]. Several reasons would push towards the design of sparse 2D arrays, which do not satisfy Nyquist's sampling limit for inter-element spacing ($\leq \lambda/2$ for a rectangular grid; where λ is the acoustic wavelength). For physical piezo-based arrays, these reasons include manufacturing and control challenges due to the large number of elements needed when satisfying Nyquist's criterion [3]. This issue is alleviated when using LIPAs, which are synthetic ultrasound arrays produced using only two lasers, one for wave generation and another for wave detection. This flexibility allows for the optimisation and easy adaptation of array designs for various applications and objectives (e.g., detection or characterisation). Additional reasons for using sparse arrays include the required time, storage, and energy when employing a large number of transmit/receive elements. Such high resource demands pose significant challenges for large-area inspections.

On the other hand, the use of sparse regular arrays can lead to aliasing in the reconstructed wavefield, resulting in localised imaging artefacts known as grating lobes (GLs) [3]. Lukacs et al. [4, 5] explored the design of sparse 2D LIPAs which can suppress GLs and prevent their constructive buildup. Several approaches were compared, including the use of rotated arrays (the detection layout is rotated from the generation one), Vernier arrays (different generation and detection pitches), and random arrays (random but same generation and detection layouts). The analytical and experimental results proved the effectiveness of random arrays in suppressing the GLs and producing better imaging results. Velichko and Wilcox [3] suggested optimising 2D arrays using a Poisson-disk (PD) distribution – one of the best known solutions for non-uniform sampling with a constraint on the minimum inter-element distance. It was shown that the PD distribution suppresses the GLs but at the cost of increased uniform noise in the image. For a noise level below -35 dB, the PD layout allowed a mean element pitch twice as the best uniform configuration (triangular/hexagonal). Since the optimised array was physical, the same element layout was used for both wave generation and detection.

This paper suggests a new approach which uses both sparse and separate Poisson-disk generation and detection layouts to efficiently scan large components using 2D LIPAs. In addition to the above-mentioned advantages, the proposed solution has several practical benefits over previous work, which can be summarised as follows:

- More flexibility due to separating the detection and generation layouts;
- Improved imaging because of the increased randomness and minimised overlap;

- Easier implementation when planning a scan, by defining the detection layout directly over the scanned surface;
- Preventing measurement repetition with ease since each scanned detection point presents unique transmit-receive combinations;
- Efficient scanning, data storage, data handling, and imaging by the separate treatment of each detection point and its corresponding generation aperture.

The rest of the paper presents the suggested scanning and imaging technique, a proposed performance-evaluation metric, and a comparison between various sensing configurations.

II. SUGGESTED SCANNING TECHNIQUE

For large-area scans, it is important to scan the required surface efficiently and effectively. Efficiency can be defined in terms of time, energy consumption, data-storage needs, and costs, while effectiveness can be defined by ensuring a uniformly high probability of detection over the whole inspected volume. This can be achieved by using the least possible number of measurements per unit area while not compromising the damage-detection performance. Hence, the overall goal is to acquire sufficient A-scan measurements from the scanned surface so that enough wave generation and detection points exist around any given point on the surface to achieve the required effectiveness. The evaluation of the imaging performance will be explained in Section IV.

The suggested approach is to define a detection layout over the surface (of any arbitrary shape), which would therefore be followed by the detection laser during the scan. At each detection position, waves are generated within a specified physical aperture of generation points around the detection point using the generation laser. Figure 1 (a) shows an example of a possible detection layout over a surface of 50×30 mm^2. The layout was defined using a Bridson Poisson-disk distribution [6] to ensure randomness while maintaining a minimum distance between the detection locations. An omnidirectional perfect point scatterer is assumed to exist beneath the surface at location (15, 0, -12) mm. The negative z direction is assumed to be into the page (through the component thickness). The provided example is for demonstration over a single generic case, and the size of the scanned surface is good enough to serve the intended study.

Figure 1(b) shows an example measurement layout of the scan, depicting the generation locations distributed within 5 mm (physical aperture) around each detection position. Figure 2 shows three of the nine generation apertures (physical apertures) compared in this study, while Figure 3 shows three out of the nine detection layouts. The comparison considered three possible distributions of detection/generation points, namely, square, triangular, and Poisson-disk. To ensure a valid comparison, all the assessed layouts contained an equal number of points over the detection/generation surface. Three physical-aperture sizes – 5 mm, 10 mm, and 25 mm – were considered, where Figure 2 illustrates the 5-mm case. Additionally, three detection-layout densities were compared by using 70, 416, and 936 detection points within the surface of interest. No mixing between distribution types was considered; therefore, a total of 27 measurement layouts were evaluated in this study. All the layouts are considered sparse since the minimum distances between the points are always maintained above half the wavelength ($\lambda/2 \approx 0.31$ mm) of the ultrasound central frequency used.

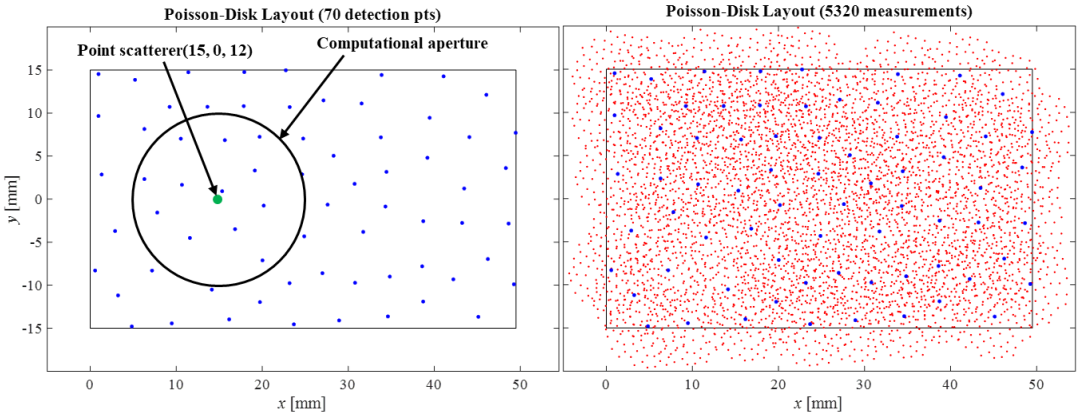

(a) (b)

Figure 1. (a) Example wave-detection layout of PD distribution defined over the geometry of the scanned surface. A point scatterer exists 12 mm below the scanned surface. A moving computational aperture is defined by a specific radius to pick the points needed for imaging at its centre; and (b) the corresponding measurement layout defined by using a chosen wave-generation layout for each point of the wave-detection layout, leading to a total of 5320 transmit-receive measurement combinations. Blue: wave-detection point; red: wave-generation point.

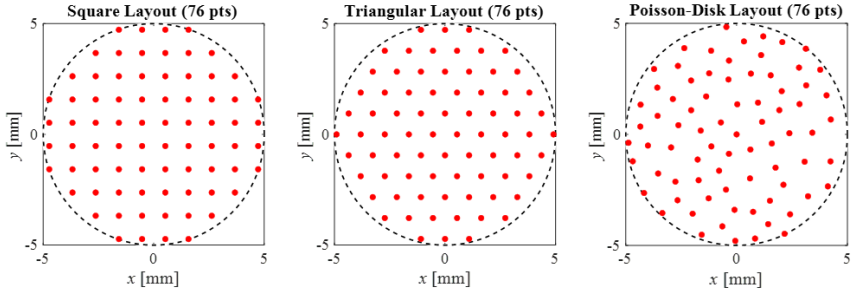

Figure 2. Three of the nine compared wave-generation layouts of square, triangular, and Poisson-disk distributions. All the layouts have the same number of points and geometry (circular). The performance of three different radii (physical apertures) is evaluated (5 mm, 10 mm, and 25 mm).

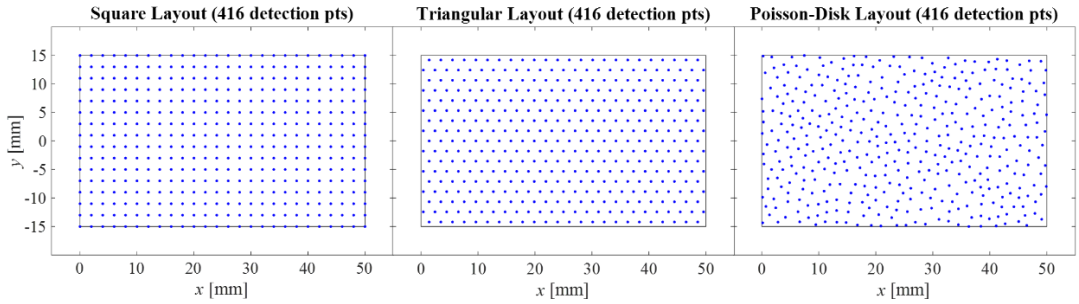

Figure 3. Three of the nine compared wave-detection layouts of square, triangular, and Poisson-disk distributions. All the layouts have the same number of points and geometry (the scanning surface). The performance of three different detection densities is evaluated (70, 416, and 936 points).

III. SIMULATION AND IMAGING

For the ultrasound simulations, a LIPA ray-tracing 3D model was used based on [7], which was developed for in-contact inspection configurations. The details of the LIPA ray-tracing 2D model and matched filter total focusing method (TFM) for imaging can be found in [2]. The same model and imaging algorithms were adopted in this work but modified for 3D models. For this purpose, a point-source directivity equation was employed instead of the line-source equation, according to [8]. Further, the beam-spread attenuation for the transmit and receive paths was calculated as $1/d$ (instead of $1/\sqrt{d}$ for the 2D case [2]), where d denotes the distance between the generation/detection point and the scatterer. The study examined an aluminium sample of the following material properties: Young's modulus $E =$ 70 GPa, Poisson's ratio $\nu = 1/3$, and density $\rho = 2700$ kg/m^3. The excitation signal used for wave generation was a 5-cycle Gaussian toneburst of central frequency $f = 5$ MHz.

The proposed imaging technique, suitable for the suggested scanning method, is distinct from the traditional and earlier LIPA techniques. A uniform (structured) volumetric imaging grid is defined for the volume of interest (under the scanned surface). For each region of interest (ROI), defined by an imaging location on the surface and all the voxels underneath, the full matrix capture (FMC) is constructed using only the detection points located within a defined area surrounding the surface point. This area is characterised by a specific radius, which determines the size of the computational aperture.

Figure 1(a) shows an example computational aperture of radius 10 mm, for the ROI where the scatterer exists. After a study of the needed size of the computational aperture for the current example (not presented here for brevity), a radius $R_{comp} = 10$ mm was chosen. However, this value cannot be generalised, and this parameter should be optimised for broader applications.

IV. PERFORMANCE EVALUATION

For simplicity and due to the symmetry of the problem (ignoring the randomness aspect), the 27 examined laser-scanning layouts were compared by visualising and evaluating their performance over a single through-thickness slice of 20 mm depth passing through the scatterer, i.e., the x-z plane ($y = 0$). Figure 4(a-c) show three imaging examples when using the three different types of sensing distributions (square, triangular, and PD), with detection layouts of 936 detection points and generation layouts of $R_{gen} = 25$ mm. The level of artefacts in the three images is considered low, as only weak artefacts (< -25 dB) appear beyond the scatterer's location. Despite the high measurement density ($\sim$47.42 measurements/mm^2), the used layouts are still considered sparse (minimum distances > $\lambda/2$). In such a case, the random distribution of the PD sensing layout shows superiority in suppressing imaging artefacts caused by the grating lobes, generally associated with regular distributions like square and triangular grids [4]. All three images show a clear indication of the scatterer; however, it is evident that the least performing layout is the square grid, followed by the triangular grid, while the PD distribution shows very minimal artefacts.

To both identify and quantify the artefact level, the main lobe was masked (Figure 4(d)), then the indications in the rest of the image were assessed. Figure 4(d) shows the

same image as that in Figure 4(b) but with a wider decibel (dB) range to see the weak level of artefacts more clearly. The mask's radius (a parameter of choice) was considered to be equal to twice the signal wavelength ($2\lambda \approx 1.25$ mm). The absolute root-mean-square (RMS) artefact level was then used for layout evaluation, according to Equations (1) and (2):

$$N_a^2 = \frac{1}{\Omega}\int_{\Omega} M(r)|P(r)|^2 dr\,; \tag{1}$$

$$M(r) = \begin{cases} 0, & d_{r-scatterer} \leq 2\lambda \\ 1, & d_{r-scatterer} > 2\lambda \end{cases}; \tag{2}$$

where N_a is the absolute RMS artefact level; r is any location at the imaging grid, defined in this case by $r(x,z)$; Ω is the area of the image region; M is the function defining the main-lobe mask; $d_{r-scatterer}$ is the distance between r and the scatterer; and $P(r)$ is the matched filter TFM image value at location r.

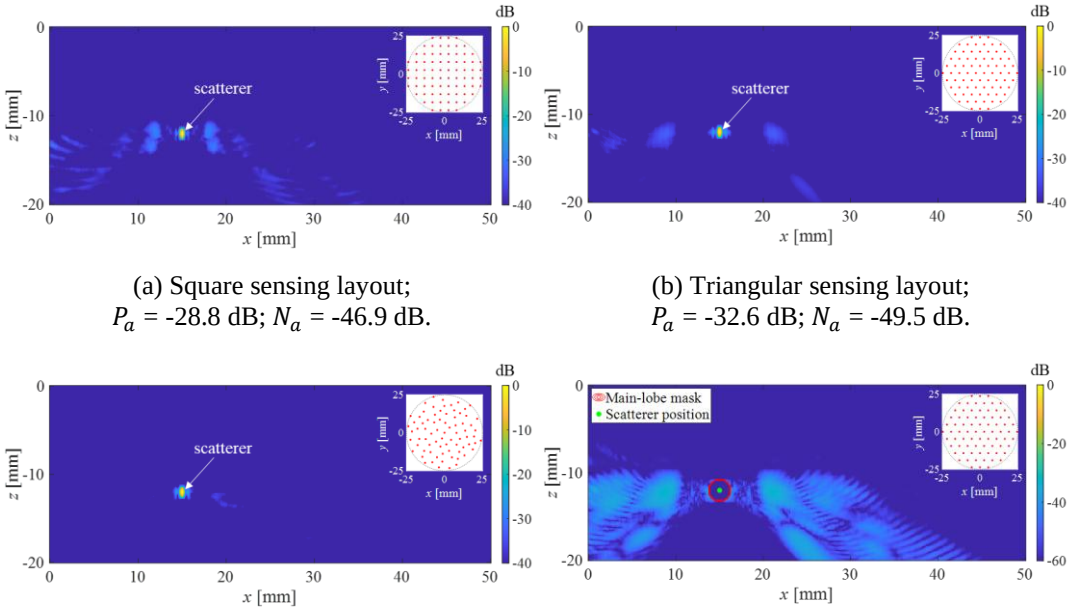

(a) Square sensing layout; P_a = -28.8 dB; N_a = -46.9 dB.

(b) Triangular sensing layout; P_a = -32.6 dB; N_a = -49.5 dB.

(c) PD sensing layout; P_a = -35.3 dB; N_a = -54.7 dB.

(d) Same image as (b) but with a larger dB scale to visualise the weaker artefacts. The scatter's location and mask, used for artefact-level evaluation, are illustrated.

Figure 4. Through-thickness normalised matched filter TFM images using three different sensing layouts. In each case, the inset shows the used 25-mm generation layout per detection point. The detection layouts of corresponding types and 936 detection points were employed.

V. RESULTS AND DISCUSSION

Figure 5 is a bar graph showing the absolute RMS artefact level for all the 27 tested measurement layouts, calculated in dB units. The vertical axis was inverted for a more intuitive comparison: a higher bar means a lower artefact level and, therefore, a better

performance. Due to the high noise levels observed in previous experiments, an artefact level of $N_a \leq$ -40 dB will be considered adequate for detection purposes.

There is an obvious improvement in the results with the increase in the number of detection points, consequently, the measurement density. The square grid is inadequate when using a very low number of measurements (70 detection points $\rightarrow \sim$3.55 measurements/mm^2). For the same measurement density, the triangular grid has an acceptable performance except for the sparsest generation layout of a physical aperture of 25 mm. On the contrary, the PD distribution shows competence even for the sparsest detection and generation layouts. This is very important for fast scans of large components to narrow down areas of uncertainty and detect possible defects. After detection, denser grids can be used for high-fidelity imaging, which is crucial for sizing and assessment.

On the other hand, for denser detection layouts and less sparse generation layouts, the superiority of the PD distribution over the triangular grid becomes less obvious, with several cases of the triangular layout slightly surpassing the performance of the PD one (5-mm generation radius with 416 detection points, and 5- and 10-mm generation radius with 936 detection points).

It was also noticed that the 5-mm generation layouts performed better than the larger aperture sizes for most of the tested cases. This, however, can change when considering a broader study comparing performances for more potential scatterer depths, types, and orientations, as was seen in [2]. Hence, a more in-depth optimisation of both the physical and computational apertures is required. Future work will also include the assessment of the robustness of various layouts to the expected high noise level, in addition to an experimental validation of the obtained results.

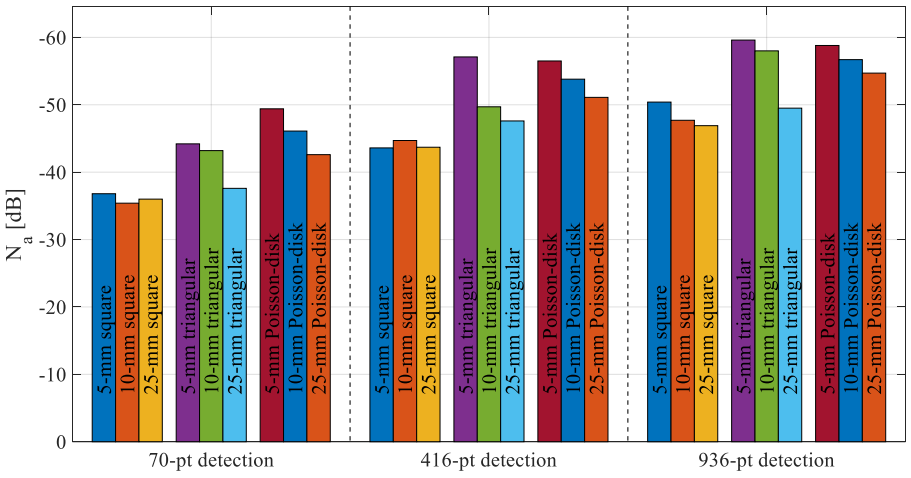

Figure 5. Absolute RMS artefact level for all the examined sensing layouts

VI. CONCLUSION

This paper proposes a methodology to optimise the scanning of large surfaces using 2D LIPAs for detection purposes, via 3D volumetric imaging. The proposed solution is to sample the surface using a Poisson-disk distribution for wave-detection locations, and define another PD wave-generation aperture to be used at each detection point. The aim

is to accomplish a target detection performance using the least possible measurement density, to reduce the scanning time, energy, and data size. The normalised matched filter TFM imaging technique is applied to the data collected from a computational aperture defined by the detection points within a specific radius around the region of interest. Square and triangular sampling layouts were compared to the proposed PD distribution using analytical ray-tracing simulations of multiple measurement densities. The layouts were evaluated based on the absolute RMS artefact level (N_a), where the PD sampling proved superior over the other sampling methods. The PD layout showed a very good potential for detection (N_a = -42.6 dB) even when using a relatively low measurement density ($\sim$3.55 measurements/mm^2). This proves the suitability of the approach for faster large-area inspections. This study gave insights for further optimisation and experimental validation in future work.

ACKNOWLEDGEMENTS

This work was supported by the UK Engineering and Physical Sciences Research Council (EPSRC) project ALIPA - Adaptive Laser Induced Phased Arrays (grant number EP/V051814/1). The authors would like to thank Dr Theodosia Stratoudaki and her team at the University of Strathclyde for their valuable discussions.

REFERENCES

1. Stratoudaki, T., M. Clark, and P.D. Wilcox, *Laser induced ultrasonic phased array using full matrix capture data acquisition and total focusing method.* Optics express, 2016. **24**(19): p. 21921-21938.
2. Cantero-Chinchilla, S., A.J. Croxford, and P.D. Wilcox, *Optimising laser-induced phased-arrays for defect detection in continuous inspections.* NDT E Int, 2024. **144**: p. 103091.
3. Velichko, A. and P.D. Wilcox. *Strategies for ultrasound imaging using two-dimensional arrays*. in *AIP Conference Proceedings*. 2010.
4. Lukacs, P., et al. *A 2D ultrasonic phased array optimization framework enabled by reconfigurable laser induced phased arrays*. in *Journal of Physics: Conference Series*. 2024. IOP Publishing.
5. Lukacs, P., et al. *Grating lobe suppression through novel, sparse laser induced phased array design*. in *2022 IEEE International Ultrasonics Symposium (IUS)*. 2022. IEEE.
6. Bridson, R., *Fast Poisson disk sampling in arbitrary dimensions.* SIGGRAPH sketches, 2007. **10**(1): p. 1.
7. Budyn, N., et al., *A model for multiview ultrasonic array inspection of small two-dimensional defects.* IEEE transactions on ultrasonics, ferroelectrics, and frequency control, 2019. **66**(6): p. 1129-1139.
8. Miller, G. and H. Pursey, *The field and radiation impedance of mechanical radiators on the free surface of a semi-infinite isotropic solid.* Proceedings of the Royal Society of London. Series A. Mathematical and Physical Sciences, 1954. **223**(1155): p. 521-541.